Article

Cell Reports

SF3B1 Association with Chromatin Determines Splicing Outcomes

Graphical Abstract

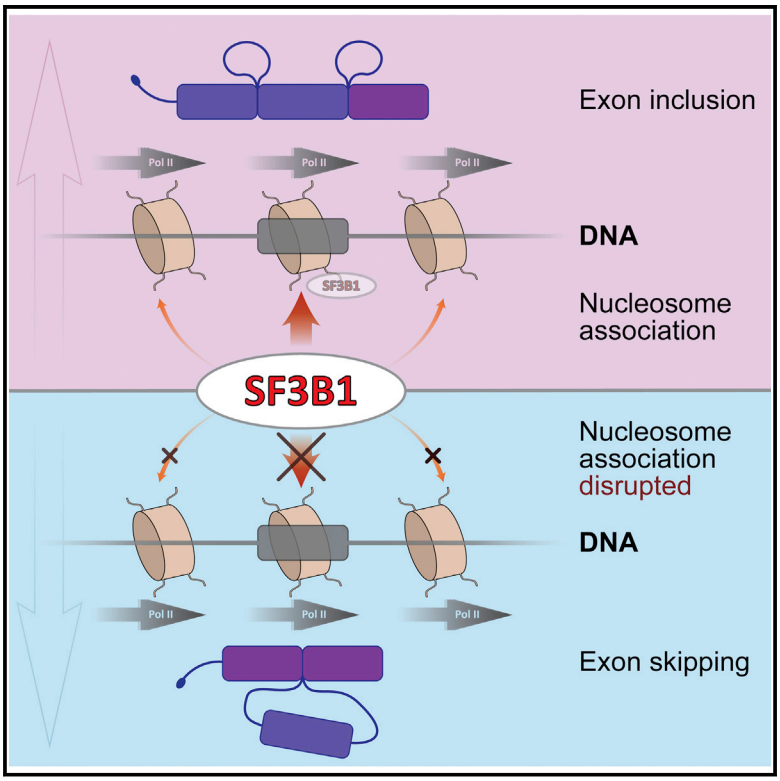

Authors

Nir Kfir, Galit Lev-Maor, ..., Eran Meshorer, Gil Ast

Correspondence

meshorer@huji.ac.il (E.M.), gilast@post.tau.ac.il (G.A.)

In Brief

The connection between mRNA splicing and chromatin composition is well established, although the precise mechanism and specific interactors remain largely unknown. Kfir et al. demonstrate that SF3B1 is associated with chromatin, specifically with nucleosomes that are located in exonic positions, and that the splicing of these exons is affected by SF3B1association.

Highlights

- Splicing factors comprising the U2 snRNP complex are associated with chromatin
- SF3B1 is associated with nucleosomes positioned over exons
- SF3B1 binding of nucleosomes facilitates the splicing recognition of exons

Accession Numbers

GSE65644

Kfir et al., 2015, Cell Reports *11*, 618–629
April 28, 2015
http://dx.doi.org/10.1016/j.celrep.2015.03.048

OPEN ACCESS
CellPress

Cell Reports
Article

SF3B1 Association with Chromatin Determines Splicing Outcomes

Nir Kfir,[1] Galit Lev-Maor,[1] Ohad Glaich,[1] Adi Alajem,[2] Arnab Datta,[4] Siu K. Sze,[4] Eran Meshorer,[2,3,5,*] and Gil Ast[1,5,*]
[1]Department of Human Molecular Genetics and Biochemistry, Sackler Faculty of Medicine, Tel-Aviv University, Ramat Aviv 69978, Israel
[2]Department of Genetics, Institute of Life Sciences, The Hebrew University of Jerusalem, Jerusalem 91904, Israel
[3]The Edmond and Lily Safra Center for Brain Sciences, The Hebrew University of Jerusalem, Jerusalem 91904, Israel
[4]School of Biological Sciences, Nanyang Technological University, 60 Nanyang Drive, Singapore 637551, Singapore
[5]Co-senior author
*Correspondence: meshorer@huji.ac.il (E.M.), gilast@post.tau.ac.il (G.A.)
http://dx.doi.org/10.1016/j.celrep.2015.03.048

SUMMARY

Much remains unknown concerning the mechanism by which the splicing machinery pinpoints short exons within intronic sequences and how splicing factors are directed to their pre-mRNA targets. One probable explanation lies in differences in chromatin organization between exons and introns. Proteomic, co-immunoprecipitation, and sedimentation analyses described here indicate that SF3B1, an essential splicing component of the U2 snRNP complex, is strongly associated with nucleosomes. ChIP-seq and RNA-seq analyses reveal that SF3B1 specifically binds nucleosomes located at exonic positions. SF3B1 binding is enriched at nucleosomes positioned over short exons flanked by long introns that are also characterized by differential GC content between exons and introns. Disruption of SF3B1 binding to such nucleosomes affects splicing of these exons similarly to *SF3B1* knockdown. Our findings suggest that the association of SF3B1 with nucleosomes is functionally important for splice-site recognition and that SF3B1 conveys splicing-relevant information embedded in chromatin structure.

INTRODUCTION

An increasing body of evidence suggests that the chromatin landscape is intrinsically intertwined with transcription and RNA processing (Alexander and Beggs, 2010; Goldstrohm et al., 2001; Keren-Shaul et al., 2013; Kornblihtt, 2006; Luco et al., 2011). These connections are evident at the very basic level of nucleosome positioning across genes and in the intricate post-transcriptional modification of nucleosome components. The connection between chromatin structure and splicing was first suggested by the discovery that nucleosomes tend to be positioned over exons rather than flanking intronic regions (Schwartz et al., 2009; Spies et al., 2009). Subsequently, it was demonstrated that trimethylation of lysine 36 on histone 3 marks exonic nucleosomes and is involved in the recruitment of splicing factors (de Almeida et al., 2011; Luco et al., 2010). Several studies have shown that splicing factors associate with histones containing specific modifications, usually via an adaptor factor that modulates the interaction (Luco et al., 2011; Schwartz and Ast, 2010). For example, the association of U2 small nuclear ribonucleoprotein particle (snRNP) components with trimethylation of lysine 4 on histone 3 is mediated through CHD1, which increases splicing efficiency (Sims et al., 2007). Other splicing machinery components, such as SR proteins and the U1 snRNP associated protein Prp40, bind to the C-terminal domain of RNA polymerase II (Pol II) during transcription (Goldstrohm et al., 2001; Morris and Greenleaf, 2000; Yuryev et al., 1996), and the elongation rate of Pol II affects splicing of certain exons (de la Mata et al., 2003; Dujardin et al., 2013). Since splicing is coupled to transcription, these observations are in line with the premise that chromatin structure, together with the transcription machinery, directs the spliceosome to exon-intron junctions, thus enabling a rapid and precise splicing process. Despite these clues, the molecular mechanisms that link chromatin architecture to the splicing machinery remain obscure.

In our exploration of the interaction between chromatin and splicing factors, we found that SF3B1 strongly associates with mononucleosomes. SF3B1 is a key component of the U2 snRNP complex; it binds the branchpoint adenosine in early stages of spliceosome assembly and facilitates the formation of the complex responsible for splicing (Gozani et al., 1998; Lardelli et al., 2010; Warkocki et al., 2009). In vitro splicing assays show that SF3B1 is required for the progression of the splicing reaction (Wang et al., 1998), and its phosphorylation is crucial for the transition to active splicing (Bessonov et al., 2010). Recently, mutations in *SF3B1* were observed in patients with hematological malignancies, and these are associated with cancer progression (Bonnal et al., 2012; Gentien et al., 2014). Three landmark publications showed that mutations in *SF3B1* that are associated with chronic lymphocytic leukemia and myelodysplastic disorders result in aberrant splicing of a sub-population of exons (Quesada et al., 2012; Wang et al., 2011; Yoshida et al., 2011). The contribution of these mutations to cancer development is not fully understood.

SF3B1 is observed in the chromatin-containing fraction of nuclear purifications (Eto et al., 2010) and interacts with chromatin remodelers (Cavellán et al., 2006; Isono et al., 2005). The Lührmann lab recently showed that the active phosphorylated form of SF3B1 is associated with chromatin via RNA (Girard et al., 2012). These data led us to focus on SF3B1 as a possible conveyer of chromatin configuration information to splicing function. In a recent study (Alajem et al., 2015), we developed an assay called differential chromatin-associated proteins (D-CAPs) for the identification of chromatin proteins that are differentially bound to chromatin in two cell types or under two sets of conditions that utilizes high-definition mass spectrometry (Dutta et al., 2012; Zhang et al., 2010). Using this assay, we found that numerous splicing factors are associated with chromatin regardless of the cell type and that a majority of these factors belong to the U2 snRNP protein complex. We further confirmed this association by direct reciprocal pull-downs of nucleosome-enriched nuclear extracts. We found that the association of SF3B1 with nucleosomes did not depend on RNA or on interactions with large protein complexes. We mapped the genome-wide positions of SF3B1-associated nucleosomes using chromatin immunoprecipitation followed by high-throughput sequencing (ChIP-seq). Our analysis shows that SF3B1-associated nucleosomes are enriched in exonic relative to flanking intronic regions. Moreover, this enrichment differed between two biologically distinct groups of exons. Examining splicing patterns by high-throughput RNA sequencing (RNA-seq) in untreated cells and cells treated with small interfering RNA (siRNA) designed to knock down *SF3B1* expression indicated that splicing of exons embedded inside SF3B1-associated nucleosomes was more often altered in SF3B1-deficient cells. Disruption of SF3B1 association with nucleosomes selectively altered the splicing pattern of the SF3B1-bound exons. Our findings provide a better understanding of the crosstalk between chromatin and splicing and suggest that SF3B1 is involved in mediating this crosstalk.

RESULTS

High-Resolution Mass Spectrometry Reveals RNA-Dependent Association of Splicing Factors with Nucleosomes

In order to identify the proteins that interact most directly with nucleosomes, we recently developed a simple biochemical method based on brief chromatin digestion with micrococcal nuclease (MNase). Briefly, nuclei purified from cells are washed four times within 150 mM KCl buffer to remove soluble nucleoplasmic proteins and proteins that are loosely bound to chromatin. Next, the nuclei are subjected to a brief MNase digestion optimized to release chromatin-associated proteins. Proteins are identified using high-definition mass spectrometry (Dutta et al., 2012; Zhang et al., 2010). This method was used to identify D-CAPs in undifferentiated mouse embryonic stem cells (ESCs) and in mouse ESCs differentiated to neuronal progenitor cells (NPCs) (Alajem et al., 2015). In this study, we were interested in chromatin association regardless of differentiation effects; therefore we used the D-CAP assay to identify proteins bound to chromatin in both ESCs and NPCs. To determine whether proteins were directly associated with chromatin or associated via RNA (e.g., through nascent transcripts being processed co-transcriptionally), we carried out the D-CAP assay in the absence or in the presence of RNase treatment. Of the proteins detected, we investigated 330 proteins that appeared in the untreated samples of both ESC and NPC cell lines (Table S1); 28 of these are known splicing factors. Figure 1 lists the chromatin-associated splicing factors grouped by function: 11 factors are part of snRNP protein complexes, four are Sm proteins auxiliary to snRNPs, seven are hnRNP proteins, three are RNA helicases, and three are splicing regulatory proteins. Strikingly, seven of the snRNP factors and one RNA helicase are known to belong to or associate with the U2 snRNP complex, and almost all are associated independently of RNA. This suggests that the U2 snRNP components bind chromatin directly, either separately or as a complex. With the exception of Snrnp200, the U1- and U5-related snRNP factors associated with chromatin in an RNA-dependent manner. Most of the hnRNPs and splicing regulatory factors showed some degree of RNA-dependent chromatin association. It was difficult to determine whether RNA-dependent associations of splicing factors with chromatin were mechanistically relevant or simply due to residual spliceosomal remnants tethered to chromatin by nascent RNA transcripts. To address this issue, we focused on the association of U2 snRNP complex with chromatin.

SF3B1 Associates with Nucleosomes Independently of RNA

To determine whether the same associations observed in ESCs and NPCs by the D-CAP assay are also present in a human cell line (HeLa), and to validate the direct association of the U2 snRNP complex with chromatin, we adopted a similar protocol to achieve a mononucleosome-enriched sample from HeLa cells. After MNase treatment, the majority of DNA fragments are 147 bp, the length of a fragment wrapped around a single nucleosome indicating an enrichment of mononucleosomes (Figure 2A). We initially immunoprecipitated histone H2B in order to pull down nucleosomes together with their associated proteins and examined the presence of SF3B1 by western blot as a measure of the amount of U2 snRNP complex. This experiment indicated a strong association of SF3B1 with H2B (Figure 2B). Then, we immunoprecipitated histone H3 and SF3B1 and probed these fractions for five different U2 snRNP components and one U1 snRNP factor (SNRPA). The U2 snRNP components displayed different degrees of association with nucleosomes, whereas SNRPA was not associated at all (Figure 2C). The factors most strongly associated with nucleosomes were SF3B1 and SF3A1, as is most apparent in the H3 pull-down untreated lane. The spliceosomal factors examined showed strong associations with SF3B1 probably as they are part of a large protein complex. The immunoprecipitation conditions were stringent and no crosslinking reagents were used, arguing that the observed interactions are biologically relevant.

We also examined whether the associations between splicing factors and nucleosomes in HeLa cells were via an RNA molecule (e.g., U2 snRNA) by performing immunoprecipitation assays with and without RNase A digestion. Equivalent amounts of

Protein	UniProt	Gene name	Chromatin association RNase: -	+
snRNP complex proteins:				
Splicing factor 3B subunit 1, 155 kDa	Q99NB9	*SF3B1*	●	●
Splicing factor 3B subunit 3, 130 kDa	Q921M3	*SF3B3*	●	●
Splicing factor 3B subunit 4, 49 kDa	Q8QZY9	*SF3B4*	●	○
Splicing factor 3A subunit 1, 120 kDa	Q8K4Z5	*SF3A1*	●	●
Splicing factor 3A subunit 3, 60 kDa	Q9D554	*SF3A3*	●	●
U2 small nuclear ribonucleoprotein A'	P57784	*SNRPA1*	●	●
U2 small nuclear ribonucleoprotein B''	Q9CQI7	*SNRPB2*	●	●
U5 small nuclear ribonucleoprotein, 200 kDa	Q69ZZ3	*SNRNP200*	●	●
U5 snRNP-specific protein, 116 kDa	Q15029	*EFTUD2*	●	○
U1 small nuclear ribonucleoprotein A	P09012	*SNRPA*	●	○
U6 snRNA-associated Sm-like protein LSm2	Q9Y333	*LSM2*	●	○
Sm proteins:				
Small nuclear ribonucleoprotein Sm D1	P62315	*SNRPD1*	●	●
Small nuclear ribonucleoprotein Sm D2	P62317	*SNRPD2*	●	●
Small nuclear ribonucleoprotein Sm D3	P62320	*SNRPD3*	●	●
Small nuclear ribonucleoprotein N	P63163	*SNRPN*	●	●
hnRNP proteins:				
Heterogeneous nuclear ribonucleoprotein A/B	Q20BD0	*HNRNPAB*	●	●
Heterogeneous nuclear ribonucleoproteins A2/B1	O88569	*HNRNPA2B1*	●	●
Heterogeneous nuclear ribonucleoproteins C1/C2	Q3U6P5	*HNRNPC*	●	●
Heterogeneous nuclear ribonucleoprotein D-like	O14979	*HNRNPDL*	●	◒
Heterogeneous nuclear ribonucleoprotein H'	P70333	*HNRNPH2*	●	◒
Heterogeneous nuclear ribonucleoprotein L	Q8R081	*HNRNPL*	●	○
Heterogeneous nuclear ribonucleoprotein M	Q9D0E1	*HNRNPM*	●	◒
RNA helicases:				
Spliceosome RNA helicase Ddx39b	Q9Z1N5	*DBX39B*	●	●
Putative pre-mRNA-splicing factor RNA helicase	O35286	*DHX15*	●	○
Pre-mRNA-processing factor 19	Q99KP6	*PRPF19*	●	◒
Splicing regulatory factors:				
Splicing factor, arginine/serine-rich 5	O35326	*SRSF5*	●	◒
Splicing factor, arginine/serine-rich 7	Q8BL97	*SRSF7*	●	◒
Splicing factor, proline- and glutamine-rich	Q8VIJ6	*SFPQ*	●	○

*Present in both cell types ●, absent in both cell types ○, absent in one cell type ◒.

Figure 1. Chromatin-Associated Splicing Factors Identified by D-CAP

Mass spectrometry results listing splicing associated factors that were identified by D-CAP assay as chromatin-associated in both cell lines: ESCs and NPCs. The right column details weather the chromatin association was maintained after RNase A digestion. The factors are grouped according to function.

SF3B1 were precipitated with anti-histone H3 antibody in the presence and absence of RNase; however, the association of SF3B3 was slightly reduced, whereas the association of SF3A1 diminished considerably and SF3B4 was entirely undetectable when samples were treated with RNase (Figure 2C). RNA digestion also reduced the extent of the association of the snRNP factors with SF3B1 to some extent, but the association of SF3B1 with H3 remained intact. Since SF3B1 exhibited a strong association with two nucleosomal proteins, we assume that it is associated with mononucleosomes. The association of SF3B1 with H3 was maintained after DNase digestion and ethidium bromide treatment eliminating the possibility of a DNA-dependent association (Figure S1). In support of this hypothesis, SF3B1 has been implicated in engaging with chromatin by several other studies (Cavellán et al., 2006; Convertini et al., 2014; Eto et al., 2010). Therefore, we focused much of our effort on investigating the role of SF3B1 as a potential mediator between splicing and chromatin.

SF3B1 Localizes with Nucleosome Complexes

We attempted to ascertain whether SF3B1 was associated with nucleosomes through a specific histone tail modification using co-immunoprecipitation (co-IP) assays and histone tail modification peptide arrays. We did not identify histone modifications that specifically correlate with SF3B1 binding (data not shown). It is possible that the nucleosomal association of SF3B1 is mediated through a large protein complex interaction; for example, the entire spliceosome may associate with the nucleosome. To evaluate this, we either mildly or extensively digested nuclei extracted from HeLa cells with MNase (Figure 3A, upper and lower panels, respectively). We then fractionated these extracts by ultra-centrifugation sedimentation on a sucrose gradient; DNA purified from each fraction was resolved by gel electrophoresis. Mild digestion with MNase led to an enrichment of polynucleosomes, whereas extensive digestion with MNase led to an enrichment of mononucleosomes. We pooled fractions containing small protein complexes and are enriched with

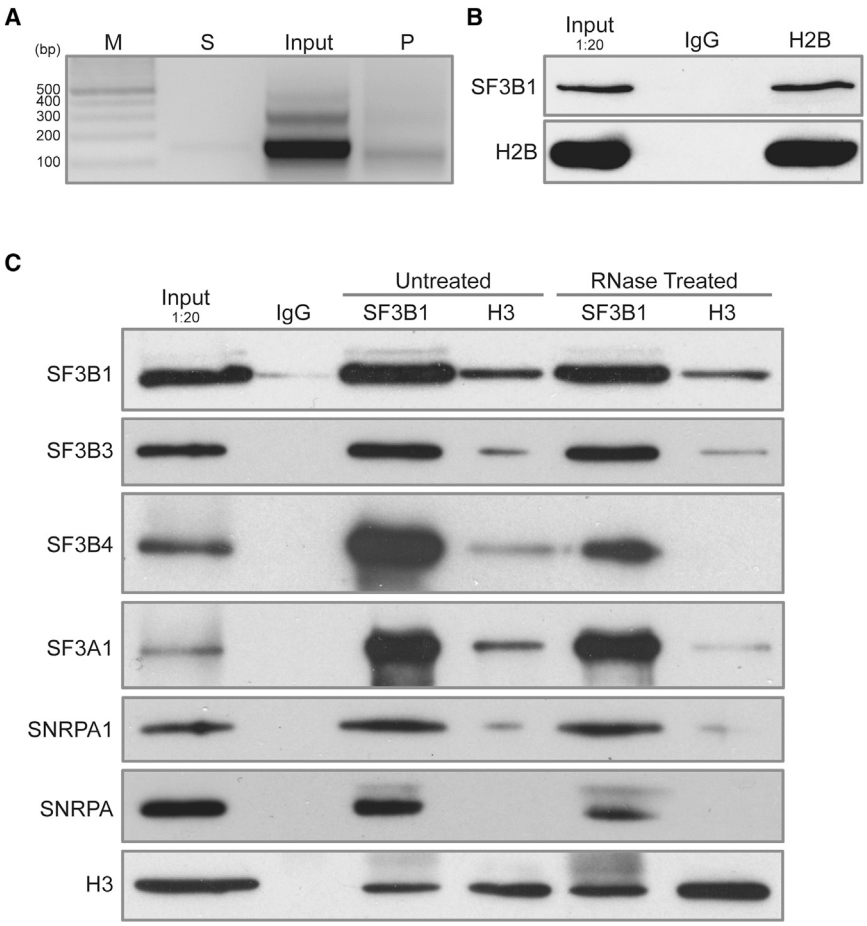

Figure 2. SF3B1 Is Associated with Nucleosomes Independently of RNA

(A) Purified HeLa cells nuclei were digested with MNase. DNA was purified from MNase digestion supernatant (lane S), soluble chromatin released to the supernatant (lane input), and nuclei pellet harboring mainly insoluble chromatin (lane P), DNA size is displayed in base-pares (lane M). Purified DNA was subjected to gel electrophoresis. DNA fragments representing mono-di-tri… nucleosome ladder.

(B) Immunoprecipitation of the mononucleosomal-enriched chromatin was performed with an anti-histone H2B antibody and a nonspecific immunoglobulin G (IgG) as control. Western blotting was performed with the indicated antibodies.

(C) Immunoprecipitation of the same input was performed with antibodies against SF3B1, histone H3, and non-specific IgG; input was either digested or not with RNase A. Western blotting was performed with the indicated antibodies.

mononucleosomes and fractions enriched with polynucleosomes that contain large protein complexes (Figure 3A, "Mono" and "Poly," respectively) and subjected the pools to RNase A treatment and co-IP. Significantly more SF3B1 was pulled down together with histone H3 in the Mono pool when these fractions were enriched with mononucleosomes and in the Poly pool when these fractions were enriched with polynucleosomes, indicating that the determining factor for the association of SF3B1 with nucleosomes is the abundance of nucleosomes (Figure 3B). Other components of the U2 snRNP complex, SF3B3 and SF3A1, did not exhibit the same phenomenon; the difference in MNase treatment did not affect their respective association with nucleosomes (Figure 3B). Without MNase digestion the sedimentation profiles of each of these three factors were similar to that of the U2 snRNP complex (Behzadnia et al., 2006) (Figure S1C). These results support the notion that SF3B1 is strongly bound to nucleosomes, but not as part of the large spliceosomal complex.

SF3B1 Is Associated with Nucleosomes Residing on Exonic DNA

Next, we sought out to determine whether SF3B1 is associated with nucleosomes positioned in specific genomic locations. Therefore, we sequenced the DNA from mononucleosome-enriched fractions (isolated as in Figure 2A) with or without immunoprecipitation with an anti-SF3B1 antibody. The sequencing yielded 81 million reads of DNA fragments wrapping mononucleosomes pulled down by SF3B1 (SF3B1) and 71 million reads of total mononucleosome-associated DNA fragments (input), 80% of which were uniquely mapped to hg18 genome assembly. The read scores on each genome coordinate of SF3B1 data were normalized to the coordinate scores of the input data to eliminate bias arising from primary chromatin landscape and to allow us to focus only on SF3B1-enriched positions. SF3B1-enriched nucleosomes were identified across the genome using HOMER software (Heinz et al., 2010) to measure the accumulation of peaks on introns, exons, and intergenic regions relative to the size of each genomic segment. This analysis showed that SF3B1 was associated mainly with nucleosomes bound to genes rather than intergenic regions and that binding of SF3B1 was enriched by 2-fold on coding exon in relation to introns (Figure 4A). As SF3B1 appears to bind preferentially to exons, it might function in the exon recognition process.

For this reason, we focused our analysis on better characterizing the associated exons, we aligned SF3B1-enriched positions on all unique exons derived from RefSeq genes (180,000 exons; Table S2) and their flanking intronic regions. We found an ~5% enrichment of SF3B1 binding on exons compared to flanking regions (Figure 4B). The observed enrichment of this analysis is different than that of genomic segment analysis (shown in Figure 4A), since it calculates the mean signal over a narrow window surrounding the splice sites and does not account for the size of the entire segment. We also examined the same data aligned to the 3′ splice site (SS) and the 5′ SS of the flanking introns and observed that SF3B1 is enriched on nucleosomes located over exonic sequences. We observed a small sub-population of

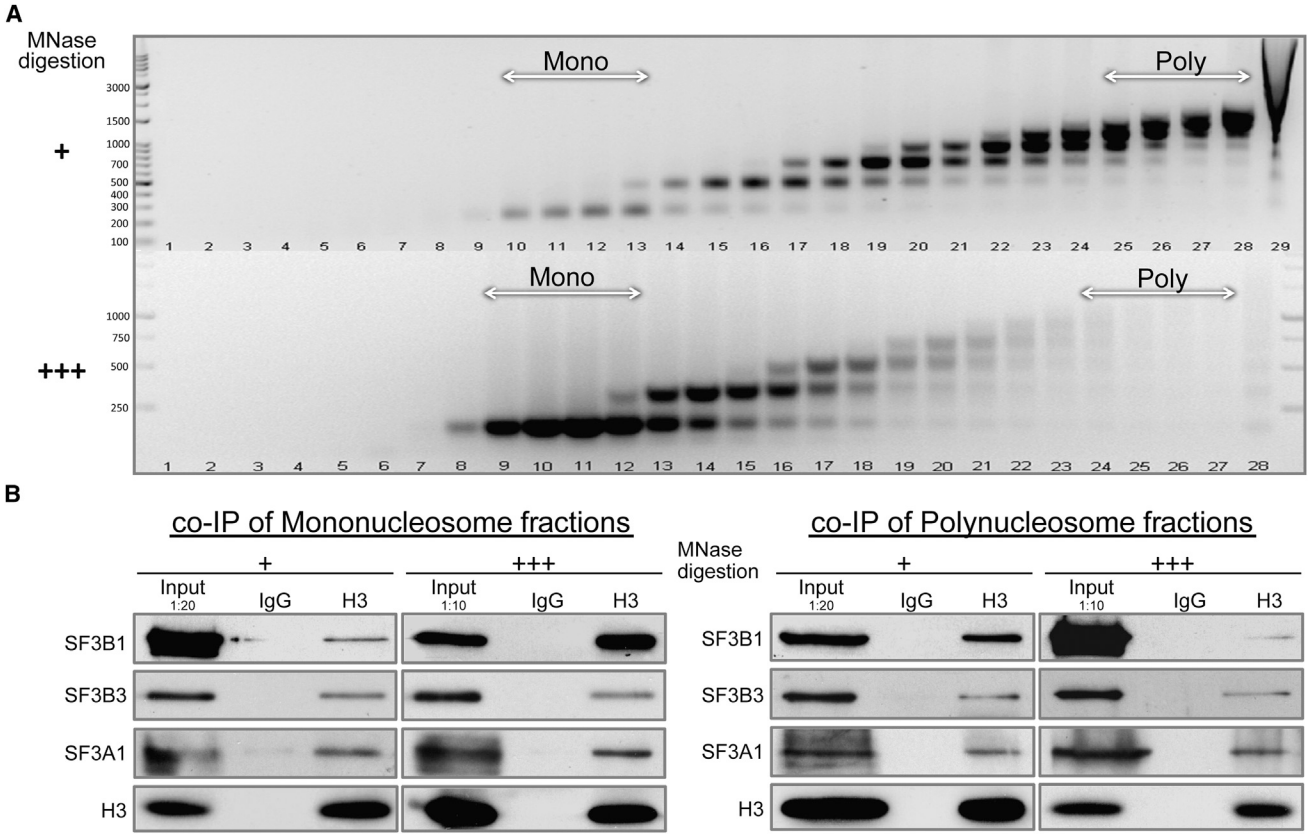

Figure 3. SF3B1 Localizes with Nucleosome Complexes

Purified nuclei from HeLa cells were digested by MNase with either 0.075 U/10^6 nuclei (+) or with 20 U/10^6 nuclei (+++), and protein complexes were separated on a 5%–25% sucrose gradient.

(A) After proteinase K digestion, DNA from each fraction was purified and subjected to gel electrophoresis.

(B) Mono (+: fractions 10-13, +++: fractions 9-12) and Poly (+: fractions 25-28, +++: fractions 24-27) fractions were pooled as indicated in (A). Each pool was immunoprecipitated with an anti-histone H3 antibody and a nonspecific IgG as control. The samples were subjected to western blotting with the indicated antibodies.

SF3B1-associated nucleosomes located slightly upstream of the 3′ SS. However, the resolution of MNase-sequencing is insufficient to identify short elements such as the branch site or the polypyrimidine track (Figures S2A and S2B).

Next, we analyzed the association of SF3B1 with exons of two different exon-intron architectures. One is a group of exons containing higher GC content than their flanking introns; these exons are characterized by long flanking introns (differential GC content). The other group of exons has similar GC content to that of their flanking introns; these exons are characterized by short flanking introns (level GC content). These two groups are recognized differently by the splicing machinery (Amit et al., 2012). In exons with differential GC content, SF3B1 was enriched by ~26% compared to the flanking regions, whereas in the level GC content group SF3B1 was enriched by ~5% (Figures 4C and 4D). We also analyzed the enrichment of SF3B1 on a group of exons that were reported to be susceptible to splicing changes due to mutations in SF3B1 that have been linked with chronic lymphocytic leukemia (Ferreira et al., 2014). The enrichment of SF3B1 on these exons in relation to flanking intronic regions is ~35%, which is significantly higher than a control of multiple random selections of the same size group (Figure 4E). Although this is a group of only 115 exons, the trend of enrichment is very clear. Taken together, these results imply that SF3B1 marks the genomic locations of short exonic sequences flanked by long intronic sequences and that the splicing regulation of some of these exons may be significant in the development and the progression of certain hematological malignancies.

We analyzed the genomic characteristics of a group of exons that are highly enriched (5-fold) with SF3B1 (701 exons) and compared these to those of a group that did not exhibit any SF3B1 enrichment. Exons were identified from clustering of the SF3B1 nucleosomal immunoprecipitation data (Figure S2C). There were no significant differences in methylation, splice-site score, or alternative/constitutive ratio between the two groups (Figures S2F–S2H). However, we found elevated H3K4me3 levels at the 3′ ends of introns upstream of SF3B1-enriched exons compared to the unenriched group (Figure S2D), although the signal is spread across a region of over 400 bp.

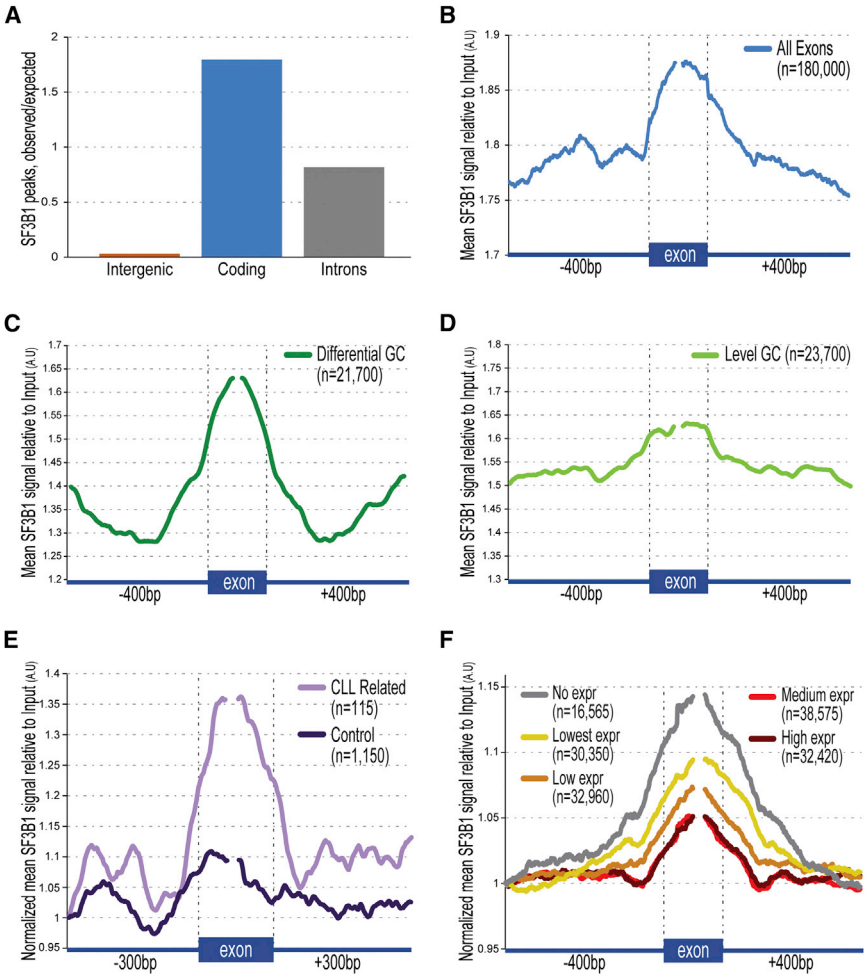

Figure 4. SF3B1 Is Associated with Nucleosomes Residing on Exonic DNA

HeLa nuclei were digested with MNase under conditions in which >90% of the DNA was cleaved into ~150-bp mononucleosomal fragments. Soluble chromatin (input) was released from the nuclei followed by RNase A digestion. DNA fragments were purified from samples immunoprecipitated with or without anti-SF3B1 antibody and subjected to deep sequencing. Fragments precipitated with anti-SF3B1 antibody and total DNA reads were mapped to the human genome (hg18 assembly).

(A) SF3B1 read peaks were normalized to input read peaks, normalized peaks that overlapped with genomic segments were identified with HOMER tools and are displayed as observed relative to expected normalized to each segment size.

(B) Normalized SF3B1/Input signal was measured across all unique exons annotated in RefSeq. The graphs in this and latter panels show the frequencies of SF3B1-bound nucleosomes on the 75-bp at exon 5′ and 3′ ends and in flanking intronic regions of sizes indicated on each graph. The frequencies are in arbitrary units (A.R.).

(C and D) Frequencies of SF3B1-bound nucleosomes on exons with (C) differential GC content and (D) level GC content.

(E) Exons derived from genes reported to show splicing changes related to SF3B1 mutations occurring in chronic lymphocytic leukemia (Ferreira et al., 2014) and in a 10× multiple random control exon group. Frequencies were normalized to the value in the first position.

(F) Exons derived from genes grouped based on expression levels. Frequencies were normalized to the value in the first position.

Error bars represent SEM.

Finally, we evaluated the enrichment of SF3B1 on exons as a function of expression level. For this purpose, we divided genes on the basis of transcript expression levels in HeLa cells obtained by RNA-seq. Exons were grouped based on the quartile of expression level of the gene they reside in. SF3B1 enrichment was most pronounced on the group of exons that were not transcribed, progressively decreased within the first three quartiles of expression, and remained the same at the two highest quartiles of expression (Figure 4F). This suggests that SF3B1 is preloaded on nucleosomes prior to transcription and that as the gene is transcribed, SF3B1 detaches from the nucleosome and likely traverses to the nascent pre-mRNA transcript. The lack of difference in SF3B1 signal between the top two quartiles of expression suggests that at a certain point, the rate of SF3B1 loading is similar to the rate of dissociation.

The Association of SF3B1 with Nucleosomes Affects Splicing

In order to determine whether the splicing of the exons tethered to nucleosomes is regulated by SF3B1, we knocked down the expression of *SF3B1* in HeLa cells by siRNA treatment (Figure 5A). We then evaluated whole-transcriptome splicing changes when SF3B1 levels were decreased by subjecting total RNA extracted from control and siRNA-treated samples to deep sequencing. We obtained 383 million paired-end reads, 80% of which were uniquely mapped to hg18 genome assembly. We identified 10,657 cassette exons with differences in inclusion by more than 10% using the SpliceTrap software (Wu et al., 2011) (Table S3). The inclusion of the majority of the affected cassette exons (92%) was decreased in SF3B1-knockdown (SF3B1-KD) cells, affirming that SF3B1 is essential for exon recognition of these alternatively spliced exons. We then evaluated 32 individual splicing events by RT-PCR; 90% were validated in trend compared to RNA-seq data analysis (Figure S3A). We also analyzed the changes in RNA expression levels between wild-type and SF3B1-KD of all components of the spliceosome as depicted by Wahl et al. and obtained from Hegele et al. (Hegele et al., 2012; Wahl et al., 2009). We found no significant changes in the expression of these genes between wild-type and SF3B1-KD (Table S4), implying that most of the changes in splicing observed are due to direct effects of SF3B1 depletion rather than to changes in expression of other genes.

Next, we examined the enrichment of SF3B1-associated nucleosomes on exons that were significantly affected by SF3B1

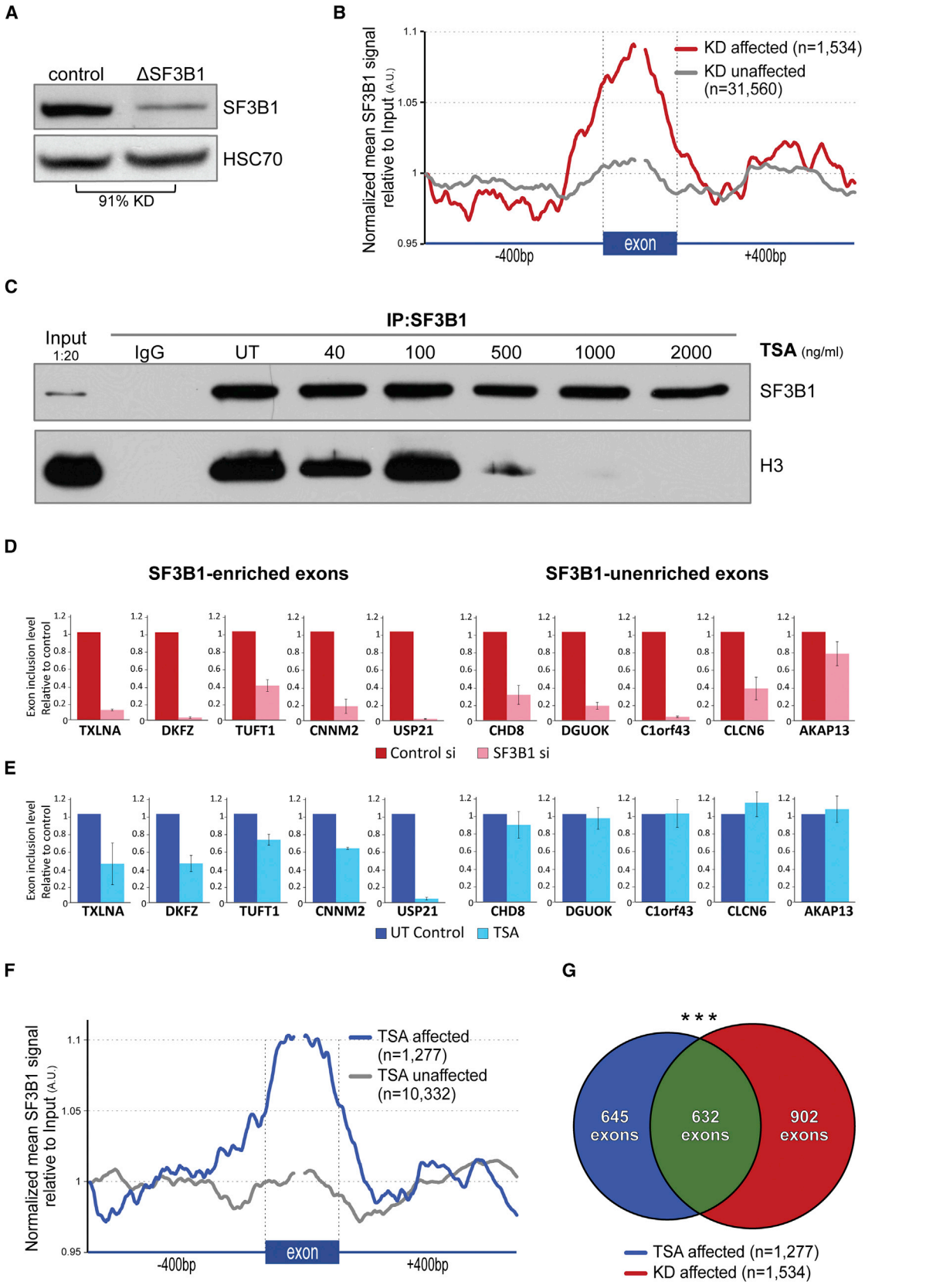

(legend on next page)

KD (over 30% change in inclusion) compared to unaffected exons (under 5% change in inclusion) (Figure 5B). Exons sensitive to diminished levels of SF3B1 were more often occupied by SF3B1-associated nucleosomes than exons that were not altered in SF3B1-deficient cells. This result implies that the coupling of SF3B1 with exonic nucleosomes is important for the splicing regulation of these exons.

To further substantiate this premise, we searched for a way to disrupt the association between SF3B1 and nucleosomes. We treated HeLa cells with chemicals known to disturb specific cellular processes. Interestingly, chemicals that alter chromatin compaction, especially histone deacetylase inhibitors, trichostatin A (TSA), sodium butyrate (NaB), and valproic acid (VPA), had the strongest effects on the SF3B1-nucleosome association (Figures S3B and S3C). TSA, which promotes histone hyperacetylation that results in chromatin relaxation (Marks et al., 2001), disrupted the co-IP of histone H3 with SF3B1 in a dose-dependent manner (Figure 5C). We also examined the association of SF3B1 with nucleosomes in HEK293 cells treated with TSA and observed the same disruption of the association as in HeLa cells (Figure S3D). We subdivided the ChIP-seq data into clusters of exons with varying SF3B1 enrichment and intersected the highly enriched and the unenriched clusters with the KD affected group of exons (Figure S4A). We measured, by qRT-PCR, the effect of TSA treatment and of treatment with siRNA targeting *SF3B1* on the splicing of ten exons: five taken from the enriched sets and five from the unenriched sets (Figures 5D and 5E). All the examined exons had decreased inclusion levels in cells treated with *SF3B1*-targeting siRNA; however, only the exons taken from the SF3B1-enriched cluster were affected by TSA. We also performed the same analysis in cells treated with two additional histone deacetylase inhibitors, NaB and VPA, and also examined the effect of DMSO (used as vehicle) and 5,6-dichlorobenzimidazole 1-β-D-ribofuranoside (DRB) (transcription inhibitor) treatments as controls. NaB and VPA had effects on splicing that were similar to those of TSA (Figure S4D). DMSO and DRB treatments had almost no effect on the tested splicing events. This further supports the idea that the association of SF3B1 with nucleosomes located on exons assists the splicing machinery in the recognition of such exons.

Next, we evaluated splicing in untreated cells and cells treated with TSA by RNA-seq. We obtained 140 million single-end reads, 60% of which were uniquely mapped to hg18 genome assembly. Using the SpliceTrap software (Wu et al., 2011), we identified 3,926 cassette exons that changed their inclusion level by more than 10% and 1,277 that displayed over 30% changes in inclusion level (Table S5), confirming the previously reported influences of TSA treatment on the splicing process (Kuhn et al., 2009; Schor et al., 2009, 2012). We examined the enrichment of SF3B1-associated nucleosomes on exons that were affected by TSA (over 30% change in inclusion) and on TSA-unaffected exons (under 5% change in inclusion) (Figure 5F). TSA preferentially affected the set of exons that were also enriched with SF3B1-bound nucleosomes: there was approximately 45% overlap between the two sets (Fisher's exact test, $p < 2.2 \times 10^{-16}$) (Figure 5G). These results support the notion that the binding of SF3B1 to a nucleosome positioned on an exon enhances the recognition of that exon by the spliceosome.

DISCUSSION

Here, we show that SF3B1, a key component of the spliceosome, is associated with mononucleosomes that are preferentially positioned over exons. Previous studies had indicated that SF3B1 is present in chromatin fractions of postnatal mouse testes (Eto et al., 2010) and that splicing factors are associated with specific histone modifications (Convertini et al., 2014; de Almeida et al., 2011; Luco et al., 2010).

Several factors belonging to the U2 snRNP complex associate with chromatin in general and specifically with histones (Sims et al., 2007). Our mass spectrometry study of chromatin-associated proteins also indicated that U2 snRNP complex components interact directly with chromatin; other spliceosomal snRNP components such as SNRPA and EFTUD2 exhibited RNA-dependent association with chromatin. A recently published analysis of proteins that interact with histone H1.0 (Kalashnikova et al., 2013) supports our observation that the association of SF3B1 with nucleosomes like that of other U2 snRNP components is not dependent on RNA. Many of the splicing factors that are associated with chromatin are related to the recognition of the branch site. This implies that when the 3′ ends of certain

Figure 5. The Association of SF3B1 with Nucleosomes Affects Splicing

(A) *SF3B1* expression was knocked down using siRNA targeting *SF3B1*; control cells were treated and with a control siRNA. Proteins were extracted and examined by western blotting with the indicated antibodies. The level of SF3B1 was quantified by ImageJ.

(B) mRNAs of siRNA-treated and control cells were analyzed using RNA-seq, and groups of affected exons (>0.3 Δ inclusion) and unaffected exons (0.05 Δ inclusion) were compiled. As in Figure 4, frequencies of SF3B1-bound nucleosomes on exons and flanking regions in the SF3B1-KD groups are displayed. Frequencies were normalized to the value in the first position.

(C) HeLa cells were treated with indicated amounts of TSA or were untreated (UT) for 16 hr. Samples were immunoprecipitated with an anti-SF3B1 antibody or nonspecific IgG as control, followed by western blotting with the indicated antibodies.

(D) Inclusion levels of ten exons were measured by qRT-PCR after treatment with *SF3B1* siRNA; data were normalized to inclusion levels in cells treated with control siRNA.

(E) Inclusion levels of the same exons were determined after treatment with 750 ng/ml TSA for 16 hr, and data were normalized to inclusion levels of untreated controls.

(F) mRNAs of TSA-treated and untreated cells were analyzed with RNA-seq. Groups of affected exons (>0.3 Δ inclusion) and unaffected exons (<0.05 Δ inclusion) were compiled. Frequencies of SF3B1-bound nucleosomes are displayed on exons and flanking regions. Frequencies were normalized to the value in the first position.

(G) Venn diagram depicts the overlap between the exons affected by SF3B1-KD and by treatment with TSA. *** denotes statistical significance of the overlap ($p < 2.2 \times 10^{-16}$).

introns emerge from Pol II, U2 snRNP moves from its location on the "exonic nucleosome" to the pre-mRNA to facilitate splicing.

In our analysis of the U2 snRNP factors bound to nucleosomes, SF3B1 was the most abundant. Since SF3B1 was not disassociated from nucleosomes by RNase digestion and sedimented together with nucleosomes, we hypothesize that SF3B1 recruits the rest of U2 snRNP complex to the nucleosome. Girard et al. showed that phosphorylated SF3B1 and the active form of Pol II are present in chromatin fractionation of HeLa nuclei, arguing that phosphorylated SF3B1 is associated with active transcription (Girard et al., 2012). In addition, they showed that association of phosphorylated SF3B1 with chromatin is RNA dependent and reaffirmed that it is the phosphorylated form of SF3B1 that is present in active spliceosome complexes (Bessonov et al., 2010). Given that we examined total SF3B1, which consists of all phosphorylation states, these results together with our findings suggest that SF3B1 phosphorylation triggers the transition of nucleosome-bound SF3B1 to nascent RNA in order to recruit the U2 snRNP complex to exons.

There is large difference in splicing dynamics in vitro and in vivo. In cell-free systems, splicing of transcripts generated by Pol II occurs over 15 to 60 min (Das et al., 2006), whereas in live cells, β-globin introns are transcribed and efficiently excised in 20–30 s (Martin et al., 2013). Two interdependent nuclear states are likely to be responsible for directing the splicing machinery and immensely improving splicing efficiency: the coupling of splicing to transcription (Listerman et al., 2006; Luco et al., 2011) and the tendency of nucleosomes to reside in exonic genomic regions (Schwartz et al., 2009). Our genome-wide analyses revealed that SF3B1 is associated with nucleosomes residing over exons. This is probably not a general phenomenon for all exons, as only a subset of exons tether nucleosomes that are highly enriched with SF3B1. We show that nucleosomes that associate with SF3B1 have an even higher exonic occupancy. Thus, SF3B1 might separate "exonic" nucleosomes from "ordinary" nucleosomes. Therefore, we suggest a mechanism in which SF3B1 traverses from an exonic nucleosome to the branch site of a nascent pre-mRNA transcript as it is being transcribed in order to facilitate the immediate and efficient recognition of that exon by the spliceosome.

However, most of the exons associated with SF3B1-bound nucleosomes have higher levels of GC content compared to their flanking intronic sequences, a characteristic most commonly observed for exons flanked by long introns (Amit et al., 2012). This implies that SF3B1 is recruited to nucleosomes for the purpose of directing the spliceosome to pertinent positions within a gene, probably prior to transcription. We observed higher levels of SF3B1 on exons that were not part of actively transcribed genes. The transcription rate of Pol II was inversely correlated with SF3B1 binding at lower levels of expression. In the two highest quartiles of expression, there were no differences in SF3B1 enrichment. This suggests that the rate of SF3B1 dissociation from the nucleosome to bind to the nascent pre-mRNA transcript is equal to rate of a SF3B1 loading on the exonic nucleosome for these highly expressed genes.

In order to elucidate why SF3B1 binds preferentially to certain exons rather than others, we used RNA-seq to compare splicing in control cells and in SF3B1-KD cells. We found that reduction in SF3B1 levels resulted in diminished splicing and a decline in the recognition of thousands of exons. Interestingly, nucleosomes coupled with SF3B1 were more abundant on exons that were most effected by SF3B1 KD. Similarly, disturbing the SF3B1-nucleosome bond resulted in the downregulation of a large number of exons that exhibited the same enrichment in SF3B1-associated nucleosomes. Moreover, the recognition of 632 exons was significantly affected by both SF3B1 KD and nucleosomal detachment, providing further evidence that regulation of splicing of a subset of exons is reliant on the proximity of SF3B1 to their genomic location.

Recently, mutations in SF3B1 have been linked to various types of cancer (Bonnal et al., 2012), and these mutations are correlated with poor prognosis in patients with chronic lymphocytic leukemia and myelodysplastic disorders (Quesada et al., 2012; Yoshida et al., 2011). Whether the pathogenesis of these mutations is a consequence of reduced levels of functional protein or dominant-negative effects remains unclear. Most reported mutations in *SF3B1* gene are located within the 22 carboxy-terminal HEAT repeats that mediate protein-protein interactions (Groves and Barford, 1999; Rossi et al., 2011; Xing et al., 2006), and thus suggest a mechanistic failure in splicing. Hence, it is feasible that these mutations disrupt the interaction of SF3B1 with nucleosomes, subsequently interfering with splicing of a group of exons and contributing to cancer progression. This idea is supported by findings that show splicing regulation is altered in subjects carrying these mutations (Wang et al., 2011) and that changes occur in relatively small groups of splicing events (Ferreira et al., 2014), similar to the effect we observe when we disturbed the association of SF3B1 with nucleosomes.

Our findings reveal that SF3B1 is a mediator that connects the splicing machinery with chromatin structure. Previous studies revealed that factors associated with U1 snRNP bind to the CTD domain of Pol II (Goldstrohm et al., 2001; McCracken et al., 1997). The "commitment complex" in which U1 binds the 5′ end of an intron together with U2 snRNP and U2AF1/2 that bind the 3′ end of that intron is likely made possible by interaction of Poll II and an exonic nucleosome characterized by an interaction with SF3B1 (Roberts et al., 1998). The Pol II complex and the exonic nucleosome each harbor complementary snRNP components, thus allowing for the speedy and accurate recognition of exons. Our data shed light on how splicing is achieved within 20–30 s in vivo.

EXPERIMENTAL PROCEDURES

Cell Maintenance

HeLa cells were cultured in DMEM with 10% fetal calf serum, 0.29 mg ml^{-1} L-glutamine, 100 U ml^{-1} penicillin, 0.1 mg ml^{-1} streptomycin, and 1 U ml^{-1} nystatin at 37°C in a humidified atmosphere with 5% CO_2.

Nuclei Isolation

Cells were trypsinized and washed with PBS, then suspended in buffer 1 (60 mM KCl, 15 mM NaCl, 5 mM $MgCl_2$, 0.1 mM EGTA, 15 mM Tris-HCl [pH 7.5]) supplemented with 0.5 mM DTT, 0.1 mM PMSF, 1× complete protease inhibitor (CPI), and incubated in 0.2% IGEPAL CA-630 (NP-40). After incubation for 10 min, residual NP-40 was cleared by centrifugation on a 1.2-M sucrose cushion.

Identification of Chromatin-Associated Proteins Identified by High-Resolution Mass Spectrometry

Nuclei freshly isolated from ESCs or NPCs were washed four times in MNase digestion buffer without MNase (10 mM Tris-HCl [pH 8], 5 mM $CaCl_2$, 150 mM KCl, 0.1 mM PMSF, and protease inhibitor cocktail 1:100), resuspended in MNase digestion buffer with or without RNase (10 ng/μl, Sigma-Aldrich), rotated for 30 min at 4°C, and centrifuged (500 × *g*, 4°C, 5 min). Nuclei were then subjected to MNase treatment (4.5 U/ml MNase, Worthington) in MNase Digestion Buffer. Reactions were stopped by adding 10× MNase stop buffer (100 mM Tris HCl [pH 7.5], 100 mM EDTA, 10 mM EGTA) followed by centrifugation (13,000 × *g*, 4°C, 10 min). Supernatants were collected and subjected to mass spectrometry analyses as described in Alajem et al., 2015 (Supplemental Experimental Procedures). To verify the MNase digestion, DNA was purified from the pellets by phenol-chloroform extraction and ethanol precipitation and electrophoresed.

MNase Digestion

Nuclei were suspended in MNase digestion buffer (0.32 M sucrose, 50 mM Tris-HCl [pH 7.5], 4 mM $MgCl_2$, 1 mM $CaCl_2$) supplemented with 0.1 mM PMSF. MNase (10 U/10^6 nuclei, Worthington) was added, and samples were incubated at 37°C for 10 min. The reaction was stopped by the addition of 1 mM EDTA. Nuclei were then sedimented by centrifugation, and nuclei and supernatant were used for experiments.

Co-IP

MNase-digested nuclei were suspended in immunoprecipitation (IP) buffer (50 mM HEPES [pH 7.6], 500 mM LiCl, 1 mM EDTA, 0.7% DOC, 1% NP-40, 0.1% SDS, 1× CPI) and rotated for 1 hr at 4°C, followed by centrifugation 10,000 × *g* for 10 min. This supernatant is denoted as "input." Indicated antibodies (4 μg) were added to each input sample and rotated overnight at 4°C. Protein A beads (50 μl, Dynabeads Invitrogen) were washed and added to each sample and rotated for 4 hr at 4°C. Beads were washed four times with IP buffer and once with 0.5 ml RNase A buffer (PBS, 0.02% Tween 20, CPI, 0.1 mM PMSF). Samples were re-suspended in 450 μl RNase A buffer and 1 μl of 10 mg/ml RNase A (Sigma-Aldrich) and incubated for 30 min at 37°C. All samples were washed another three times with 0.5 ml IP buffer. Protein was eluted from the beads by adding 100 μl PBS and 20 μl 6× SDS sample buffer (272 mM Tris-HCl [pH 6.8], 30% glycerol, 12% SDS, 20% β-mercaptoethanol, 0.01% bromophenol blue) and incubating in a thermo-shaker for 15 min at 75°C with vigorous shaking. The supernatant was moved to a new tube and boiled for 5 min at 100°C.

Western Blots and Antibodies

Proteins were separated by SDS-PAGE on 4%–20% polyacrylamide gradient gels and transferred to 0.45-μm nitrocellulose membranes (Whatman Protran). The membranes were incubated with the appropriate primary and secondary antibodies and washed with TBS-Tween 20. Horseradish-peroxidase-conjugated secondary antibodies were detected by SuperSignal West Pico Chemiluminescent Substrate (Thermo Scientific PI-34080). Antibodies used were anti-SAP155 (MBL; D221-3), anti-H3 (Abcam; ab1791), anti-H2B (Abcam; ab1790), anti-SF3B4 (Abcam; ab11803), anti-SF3B3 (Proteintech; 14577), anti-SF3A1 (Proteintech; 15858), anti-SNRPA1 (Proteintech; 17368), anti-SNRPA (Santa Cruz; sc-376027), anti HSC-70 (Santa Cruz; sc-7298), donkey anti-rabbit (Abcam; ab97064), and goat anti-mouse immunoglobulin G (Abcam; ab7068).

MNase Digestion and Sucrose Density Gradient Centrifugation

Purified nuclei (1 × 10^8) resuspended in 1 ml of RSB buffer containing 0.25 M sucrose, 3 mM $CaCl_2$, and 100 μM were digested with 5 U of MNase for partial digestion or with 500 U of MNase for maximum digestion for 15 min at 37°C, and then the reaction was stopped with EDTA and EGTA (to 10 mM final concentrations). After centrifugation at 3,500 × *g* for 5 min, the nuclear pellet was resuspended in 0.3 ml of buffer (10 mM Tris-HCl [pH 7.4], 300 mM NaCl, 5 mM EDTA, 5 mM EGTA), gently rocked for 1 hr at 4°C, and centrifuged to obtain soluble nucleosomes, which were then fractionated through a sucrose density gradient solution (5 to 25% sucrose, 10 mM Tris-HCl [pH 7.4], 0.25 mM EDTA) containing the indicated concentrations of NaCl at 100,000 × *g* for 16 hr at 4°C as described by Jeong et al. (2009)

RNA Isolation and RT-PCR Amplification

Cells were harvested using TRI reagent (Sigma-Aldrich), followed by total RNA extraction. RT-PCR was performed with SuperScript III (Life Technologies) using oligo(dT) reverse primer followed by PCR with Biotools Taq polymerase and primers complementary to flanking exon (for a list of primers, see Table S5). qPCR was performed using KAPA SYBR FAST Universal qPCR kit (KAPA Biosystems) according to the manufacturer's instructions using different exon-exon junction primer pairs to amplify the inclusion isoform and the skipping isoform. To calculate inclusion level changes upon treatment of cells with SF3B1 siRNA we used the following equation: $2^{inclusionCt(control)-inclusionCt(knockdown)}/2^{skippingCt(control)-skippingCt(knockdown)}$. All qPCR reactions were run on a Stratagene Mx3005P thermocycler. Individual primer sequences are listed in Table S6.

siRNA Treatment

HeLa cells were grown in 3.5-cm plates to a confluence of 40%. Cells were transfected with 20 nM of a control nontargeting siRNA (Thermo Scientific, D-001206) or with SF3B1 targeting siRNA (Thermo Scientific, D-020061) for 48 hr using Lipofectamine RNAiMAX transfection reagent (Invitrogen).

Deep Sequencing and Data Analysis

All of the library preparation and deep sequencing was performed by the Technion Genome Center on the Illumina HiSeq 2000. For ChIP-seq, MNase-digested DNA fragments (~150 bp in size) of SF3B1 pull down and of input samples were sequenced by single-end 50-bp reads. Reads from both samples were aligned to hg18 genome assembly using Bowtie software in default parameters (Langmead et al., 2009). Each read was denoted a single score 75 bp from the start of the read, thus marking a single position as the center of the fragment/nucleosome. Peak distribution was analyzed by HOMER tools findPeaks.pl and anotatePeaks.pl, and calculated as the ratio of observed to expected for each entity (Heinz et al., 2010). Data were then cast upon RefSeq annotated coordinates of all known exons and 400 bp of respective flanking regions as described by Gelfman et al. (Gelfman et al., 2013). Each center nucleosome score was expanded 73 bp upstream and downstream, creating 147-bp segments representing a nucleosome-binding site. The superposition of scores resulted in nucleosome occupancy peaks across the exon-intron structure. Scores of each position were averaged in the relevant group of exons (e.g., all exons, differential GC, level GC, cancer). Next, we applied a running average of 20-nt windows on the vector of average values for the exon-intron structure. The average nucleosome occupancy of SF3B1 sample was normalized to that of the input sample.

Differential and level GC content groups were compiled as described by Gelfman et al. (Gelfman et al., 2013). In brief, we tagged the locations of G and C nucleotides across the genome. Next, we measured the GC percentage of each exon in our list of all known exons derived from RefSeq. We also measured the GC percentage of 500-bp segments upstream and downstream of every exon. We performed a chi-square statistical test on data for each segment to determine whether the GC content of a given exon was significantly higher than that of flanking regions ($p < 0.05$). This test yielded a group of 21,697 exons with differential GC content and a group of 23,696 exons with level GC content. SF3B1 enrichment was calculated in each group as described for the "all exons" group.

For RNA-seq, total RNA was extracted from siRNA-treated and control cells. RNA quality was determined by gel electrophoresis. mRNA was isolated using poly(A) selection. Sequencing was performed using 100-bp paired-end reads from SF3B1-KD and control cells and using 50-bp single-end reads of TSA-treated and untreated cells. Approximately 260 million reads were obtained for each end of each sample in high quality as determined by FastQC software. Reads were aligned to hg18 genome assembly using Bowtie software with default parameters, and splicing analysis was performed using SpliceTrap (v0.90.5) software with default parameters (Cutoff-M, Junction reads-5) (Wu et al., 2011). SpliceChange software was employed to determine splicing changes between samples using default parameters.

ACCESSION NUMBERS

All of the generated databases, including raw and processed data, have been deposited to the NCBI GEO and are available under accession number GSE65644.

SUPPLEMENTAL INFORMATION

Supplemental Information includes Supplemental Results, Supplemental Experimental Procedures, four figures, and six tables and can be found with this article online at http://dx.doi.org/10.1016/j.celrep.2015.03.048.

ACKNOWLEDGMENTS

We thank Prof. Juan Valcarcel for comments and critical reading of the manuscript. We thank Mr. Dror Hollander scientific and statistical advice. G.A. was funded by grants from the Israel Science Foundation (ISF-BIkura 838/10, ISF 61/09), the Israel Cancer Association, and the Israel Cancer Research Foundation. E.M. was supported by the Israel Science Foundation FIRST individual grant (ISF 1430/13), the Israel Science Foundation (ISF 1252/12, 657/12), the Abisch-Frenkel Foundation, and the European Research Council FP7 grant (ERC-281781). The funders had no role in study design, data collection and analysis, decision to publish, or preparation of the manuscript.

Received: July 27, 2014
Revised: February 25, 2015
Accepted: March 22, 2015
Published: April 16, 2015

REFERENCES

Alajem, A., Biran, A., Harikumar, A., Sailaja, B.S., Aaronson, Y., Livyatan, I., Nissim-Rafinia, M., Sommer, A.G., Mostoslavsky, G., Gerbasi, V.R., et al. (2015). Differential association of chromatin proteins identifies BAF60a/SMARCD1 as a regulator of embryonic stem cell differentiation. Cell Rep. *10*, 2019–2031.

Alexander, R., and Beggs, J.D. (2010). Cross-talk in transcription, splicing and chromatin: who makes the first call? Biochem. Soc. Trans. *38*, 1251–1256.

Amit, M., Donyo, M., Hollander, D., Goren, A., Kim, E., Gelfman, S., Lev-Maor, G., Burstein, D., Schwartz, S., Postolsky, B., et al. (2012). Differential GC content between exons and introns establishes distinct strategies of splice-site recognition. Cell Rep. *1*, 543–556.

Behzadnia, N., Hartmuth, K., Will, C.L., and Lührmann, R. (2006). Functional spliceosomal A complexes can be assembled in vitro in the absence of a penta-snRNP. RNA *12*, 1738–1746.

Bessonov, S., Anokhina, M., Krasauskas, A., Golas, M.M., Sander, B., Will, C.L., Urlaub, H., Stark, H., and Lührmann, R. (2010). Characterization of purified human Bact spliceosomal complexes reveals compositional and morphological changes during spliceosome activation and first step catalysis. RNA *16*, 2384–2403.

Bonnal, S., Vigevani, L., and Valcárcel, J. (2012). The spliceosome as a target of novel antitumour drugs. Nat. Rev. Drug Discov. *11*, 847–859.

Cavellán, E., Asp, P., Percipalle, P., and Farrants, A.K. (2006). The WSTF-SNF2h chromatin remodeling complex interacts with several nuclear proteins in transcription. J. Biol. Chem. *281*, 16264–16271.

Convertini, P., Shen, M., Potter, P.M., Palacios, G., Lagisetti, C., de la Grange, P., Horbinski, C., Fondufe-Mittendorf, Y.N., Webb, T.R., and Stamm, S. (2014). Sudemycin E influences alternative splicing and changes chromatin modifications. Nucleic Acids Res. *42*, 4947–4961.

Das, R., Dufu, K., Romney, B., Feldt, M., Elenko, M., and Reed, R. (2006). Functional coupling of RNAP II transcription to spliceosome assembly. Genes Dev. *20*, 1100–1109.

de Almeida, S.F., Grosso, A.R., Koch, F., Fenouil, R., Carvalho, S., Andrade, J., Levezinho, H., Gut, M., Eick, D., Gut, I., et al. (2011). Splicing enhances recruitment of methyltransferase HYPB/Setd2 and methylation of histone H3 Lys36. Nat. Struct. Mol. Biol. *18*, 977–983.

de la Mata, M., Alonso, C.R., Kadener, S., Fededa, J.P., Blaustein, M., Pelisch, F., Cramer, P., Bentley, D., and Kornblihtt, A.R. (2003). A slow RNA polymerase II affects alternative splicing in vivo. Mol. Cell *12*, 525–532.

Dujardin, G., Lafaille, C., Petrillo, E., Buggiano, V., Gómez Acuña, L.I., Fiszbein, A., Godoy Herz, M.A., Nieto Moreno, N., Muñoz, M.J., Alló, M., et al. (2013). Transcriptional elongation and alternative splicing. Biochim. Biophys. Acta *1829*, 134–140.

Dutta, B., Adav, S.S., Koh, C.G., Lim, S.K., Meshorer, E., and Sze, S.K. (2012). Elucidating the temporal dynamics of chromatin-associated protein release upon DNA digestion by quantitative proteomic approach. J. Proteomics *75*, 5493–5506.

Eto, K., Sonoda, Y., Jin, Y., and Abe, S. (2010). Phosphorylated SAP155, the spliceosomal component, is localized to chromatin in postnatal mouse testes. Biochem. Biophys. Res. Commun. *393*, 577–581.

Ferreira, P.G., Jares, P., Rico, D., Gómez-López, G., Martínez-Trillos, A., Villamor, N., Ecker, S., González-Pérez, A., Knowles, D.G., Monlong, J., et al. (2014). Transcriptome characterization by RNA sequencing identifies a major molecular and clinical subdivision in chronic lymphocytic leukemia. Genome Res. *24*, 212–226.

Gelfman, S., Cohen, N., Yearim, A., and Ast, G. (2013). DNA-methylation effect on cotranscriptional splicing is dependent on GC architecture of the exon-intron structure. Genome Res. *23*, 789–799.

Gentien, D., Kosmider, O., Nguyen-Khac, F., Albaud, B., Rapinat, A., Dumont, A.G., Damm, F., Popova, T., Marais, R., Fontenay, M., et al. (2014). A common alternative splicing signature is associated with SF3B1 mutations in malignancies from different cell lineages. Leukemia *28*, 1355–1357.

Girard, C., Will, C.L., Peng, J., Makarov, E.M., Kastner, B., Lemm, I., Urlaub, H., Hartmuth, K., and Lührmann, R. (2012). Post-transcriptional spliceosomes are retained in nuclear speckles until splicing completion. Nat. Commun. *3*, 994.

Goldstrohm, A.C., Greenleaf, A.L., and Garcia-Blanco, M.A. (2001). Co-transcriptional splicing of pre-messenger RNAs: considerations for the mechanism of alternative splicing. Gene *277*, 31–47.

Gozani, O., Potashkin, J., and Reed, R. (1998). A potential role for U2AF-SAP 155 interactions in recruiting U2 snRNP to the branch site. Mol. Cell. Biol. *18*, 4752–4760.

Groves, M.R., and Barford, D. (1999). Topological characteristics of helical repeat proteins. Curr. Opin. Struct. Biol. *9*, 383–389.

Hegele, A., Kamburov, A., Grossmann, A., Sourlis, C., Wowro, S., Weimann, M., Will, C.L., Pena, V., Lührmann, R., and Stelzl, U. (2012). Dynamic protein-protein interaction wiring of the human spliceosome. Mol. Cell *45*, 567–580.

Heinz, S., Benner, C., Spann, N., Bertolino, E., Lin, Y.C., Laslo, P., Cheng, J.X., Murre, C., Singh, H., and Glass, C.K. (2010). Simple combinations of lineage-determining transcription factors prime cis-regulatory elements required for macrophage and B cell identities. Mol. Cell *38*, 576–589.

Isono, K., Mizutani-Koseki, Y., Komori, T., Schmidt-Zachmann, M.S., and Koseki, H. (2005). Mammalian polycomb-mediated repression of Hox genes requires the essential spliceosomal protein Sf3b1. Genes Dev. *19*, 536–541.

Jeong, S., Liang, G., Sharma, S., Lin, J.C., Choi, S.H., Han, H., Yoo, C.B., Egger, G., Yang, A.S., and Jones, P.A. (2009). Selective anchoring of DNA methyltransferases 3A and 3B to nucleosomes containing methylated DNA. Mol. Cell. Biol. *29*, 5366–5376.

Kalashnikova, A.A., Winkler, D.D., McBryant, S.J., Henderson, R.K., Herman, J.A., DeLuca, J.G., Luger, K., Prenni, J.E., and Hansen, J.C. (2013). Linker histone H1.0 interacts with an extensive network of proteins found in the nucleolus. Nucleic Acids Res. *41*, 4026–4035.

Keren-Shaul, H., Lev-Maor, G., and Ast, G. (2013). Pre-mRNA splicing is a determinant of nucleosome organization. PLoS ONE *8*, e53506.

Kornblihtt, A.R. (2006). Chromatin, transcript elongation and alternative splicing. Nat. Struct. Mol. Biol. *13*, 5–7.

Kuhn, A.N., van Santen, M.A., Schwienhorst, A., Urlaub, H., and Lührmann, R. (2009). Stalling of spliceosome assembly at distinct stages by small-molecule inhibitors of protein acetylation and deacetylation. RNA *15*, 153–175.

Langmead, B., Trapnell, C., Pop, M., and Salzberg, S.L. (2009). Ultrafast and memory-efficient alignment of short DNA sequences to the human genome. Genome Biol. *10*, R25.

Lardelli, R.M., Thompson, J.X., Yates, J.R., 3rd, and Stevens, S.W. (2010). Release of SF3 from the intron branchpoint activates the first step of pre-mRNA splicing. RNA *16*, 516–528.

Listerman, I., Sapra, A.K., and Neugebauer, K.M. (2006). Cotranscriptional coupling of splicing factor recruitment and precursor messenger RNA splicing in mammalian cells. Nat. Struct. Mol. Biol. *13*, 815–822.

Luco, R.F., Pan, Q., Tominaga, K., Blencowe, B.J., Pereira-Smith, O.M., and Misteli, T. (2010). Regulation of alternative splicing by histone modifications. Science *327*, 996–1000.

Luco, R.F., Allo, M., Schor, I.E., Kornblihtt, A.R., and Misteli, T. (2011). Epigenetics in alternative pre-mRNA splicing. Cell *144*, 16–26.

Marks, P.A., Richon, V.M., Breslow, R., and Rifkind, R.A. (2001). Histone deacetylase inhibitors as new cancer drugs. Curr. Opin. Oncol. *13*, 477–483.

Martin, R.M., Rino, J., Carvalho, C., Kirchhausen, T., and Carmo-Fonseca, M. (2013). Live-cell visualization of pre-mRNA splicing with single-molecule sensitivity. Cell Rep. *4*, 1144–1155.

McCracken, S., Fong, N., Yankulov, K., Ballantyne, S., Pan, G., Greenblatt, J., Patterson, S.D., Wickens, M., and Bentley, D.L. (1997). The C-terminal domain of RNA polymerase II couples mRNA processing to transcription. Nature *385*, 357–361.

Morris, D.P., and Greenleaf, A.L. (2000). The splicing factor, Prp40, binds the phosphorylated carboxyl-terminal domain of RNA polymerase II. J. Biol. Chem. *275*, 39935–39943.

Quesada, V., Conde, L., Villamor, N., Ordóñez, G.R., Jares, P., Bassaganyas, L., Ramsay, A.J., Beà, S., Pinyol, M., Martínez-Trillos, A., et al. (2012). Exome sequencing identifies recurrent mutations of the splicing factor SF3B1 gene in chronic lymphocytic leukemia. Nat. Genet. *44*, 47–52.

Roberts, G.C., Gooding, C., Mak, H.Y., Proudfoot, N.J., and Smith, C.W. (1998). Co-transcriptional commitment to alternative splice site selection. Nucleic Acids Res. *26*, 5568–5572.

Rossi, D., Bruscaggin, A., Spina, V., Rasi, S., Khiabanian, H., Messina, M., Fangazio, M., Vaisitti, T., Monti, S., Chiaretti, S., et al. (2011). Mutations of the SF3B1 splicing factor in chronic lymphocytic leukemia: association with progression and fludarabine-refractoriness. Blood *118*, 6904–6908.

Schor, I.E., Rascovan, N., Pelisch, F., Alló, M., and Kornblihtt, A.R. (2009). Neuronal cell depolarization induces intragenic chromatin modifications affecting NCAM alternative splicing. Proc. Natl. Acad. Sci. USA *106*, 4325–4330.

Schor, I.E., Llères, D., Risso, G.J., Pawellek, A., Ule, J., Lamond, A.I., and Kornblihtt, A.R. (2012). Perturbation of chromatin structure globally affects localization and recruitment of splicing factors. PLoS ONE *7*, e48084.

Schwartz, S., and Ast, G. (2010). Chromatin density and splicing destiny: on the cross-talk between chromatin structure and splicing. EMBO J. *29*, 1629–1636.

Schwartz, S., Meshorer, E., and Ast, G. (2009). Chromatin organization marks exon-intron structure. Nat. Struct. Mol. Biol. *16*, 990–995.

Sims, R.J., 3rd, Millhouse, S., Chen, C.F., Lewis, B.A., Erdjument-Bromage, H., Tempst, P., Manley, J.L., and Reinberg, D. (2007). Recognition of trimethylated histone H3 lysine 4 facilitates the recruitment of transcription postinitiation factors and pre-mRNA splicing. Mol. Cell *28*, 665–676.

Spies, N., Nielsen, C.B., Padgett, R.A., and Burge, C.B. (2009). Biased chromatin signatures around polyadenylation sites and exons. Mol. Cell *36*, 245–254.

Wahl, M.C., Will, C.L., and Lührmann, R. (2009). The spliceosome: design principles of a dynamic RNP machine. Cell *136*, 701–718.

Wang, C., Chua, K., Seghezzi, W., Lees, E., Gozani, O., and Reed, R. (1998). Phosphorylation of spliceosomal protein SAP 155 coupled with splicing catalysis. Genes Dev. *12*, 1409–1414.

Wang, L., Lawrence, M.S., Wan, Y., Stojanov, P., Sougnez, C., Stevenson, K., Werner, L., Sivachenko, A., DeLuca, D.S., Zhang, L., et al. (2011). SF3B1 and other novel cancer genes in chronic lymphocytic leukemia. N. Engl. J. Med. *365*, 2497–2506.

Warkocki, Z., Odenwälder, P., Schmitzová, J., Platzmann, F., Stark, H., Urlaub, H., Ficner, R., Fabrizio, P., and Lührmann, R. (2009). Reconstitution of both steps of Saccharomyces cerevisiae splicing with purified spliceosomal components. Nat. Struct. Mol. Biol. *16*, 1237–1243.

Wu, J., Akerman, M., Sun, S., McCombie, W.R., Krainer, A.R., and Zhang, M.Q. (2011). SpliceTrap: a method to quantify alternative splicing under single cellular conditions. Bioinformatics *27*, 3010–3016.

Xing, Y., Xu, Y., Chen, Y., Jeffrey, P.D., Chao, Y., Lin, Z., Li, Z., Strack, S., Stock, J.B., and Shi, Y. (2006). Structure of protein phosphatase 2A core enzyme bound to tumor-inducing toxins. Cell *127*, 341–353.

Yoshida, K., Sanada, M., Shiraishi, Y., Nowak, D., Nagata, Y., Yamamoto, R., Sato, Y., Sato-Otsubo, A., Kon, A., Nagasaki, M., et al. (2011). Frequent pathway mutations of splicing machinery in myelodysplasia. Nature *478*, 64–69.

Yuryev, A., Patturajan, M., Litingtung, Y., Joshi, R.V., Gentile, C., Gebara, M., and Corden, J.L. (1996). The C-terminal domain of the largest subunit of RNA polymerase II interacts with a novel set of serine/arginine-rich proteins. Proc. Natl. Acad. Sci. USA *93*, 6975–6980.

Zhang, H., Guo, T., Li, X., Datta, A., Park, J.E., Yang, J., Lim, S.K., Tam, J.P., and Sze, S.K. (2010). Simultaneous characterization of glyco- and phosphoproteomes of mouse brain membrane proteome with electrostatic repulsion hydrophilic interaction chromatography. Mol. Cell. Proteomics *9*, 635–647.